TÜBİTAK

Turkish J. Eng. Env. Sci.
34 (2010) , 155 – 170.

doi:10.3906/muh-0910-59

Hydrodynamic characteristics of high speed planing hulls, including trim effects

Ahmad Reza KOHANSAL, Hassan GHASSEMI, Mahmoud GHAISI
Department of Marine Technology, Amirkabir University of Technology, Hafez Ave., 15875-4413, Tehran-IRAN
e-mail: gasemi@aut.ac.ir

Received 21.10.2009

Abstract

The main objective of this work was to introduce and validate an appropriate algorithm for studying the hydrodynamic characteristics (i.e. pressure distribution, lift, drag, and wave pattern) of 3D planing hulls and wedge-shapes, including trim effects, moving at a constant speed on the surface of calm water. The work builds on the earlier work of the authors, paying more attention to wave pattern analysis. An integral equation was derived from Green's theorem and the unknown pressure distributions on each element were determined by solving an integral equation relating the potentials on the planing hull and the free surface. The hydrodynamic characteristics of the planing hull were calculated numerically in different wetted length-to-beam ratios, deadrise angles, trim angles, and Froude numbers. The effect of spray during planing was considered in the computations of numerical results. Computational results are presented and compared with existing theories and experiments. It is shown that the agreement between the results of experimental measurements and those of the present numerical method is satisfactory.

Key Words: Planing hulls, wedge-shape, boundary element method, free surface, trim effect, wave pattern

Introduction

The planing hull form remains one of the most effective concepts for high-speed marine vehicles that are employed in commercial, military, and recreational activities. Prediction of the forces acting on a planing hull is required for hull form design. Preliminary lift and drag estimation must also be performed in the early stages of the designing process in order to estimate the propulsor and main engine's characteristics. Although the model tests present the most comprehensive analysis of hydrodynamics, they are expensive and time-consuming. Therefore, the computational procedures are the best substitute that can quickly take into account more design alternatives.

During the early part of the 20th century, the improvement of sea planes caused significant scientific concentration on the analysis of the planing hull. Many theoretical attempts have been made, and each method has proved to possess advantages and disadvantages. Dawson (1977) employed a distribution of Rankine-type sources on the ship hull and free surface. Cao et al. (1991) described a desingularized boundary integral method for fully nonlinear free-surface problems. Nakos and Sclavounos (1994) computed steady wave patterns and wave drag of several ship hulls, including transom-stern ships, with a new Rankine panel method. To calculate the

wave-making drag of catamarans, Lee and Joo (1996) used a mixed source and doublet distribution on the body surface and source distribution on the free surface. Zhao et al. (1997) introduced the strip theory for steady planing in calm water. An IBEM (Rankine panel) to solve the flow around surface-piercing hydrofoils and ships was presented by Hsin and Chou (1998). Yasko (1998) presented 2 iterative procedures for small and large Froude numbers for fully submerged 2D hydrofoils under a free surface. Janson (1997) applied linear and nonlinear potential flow calculations of free surface waves, including lift and induced drag of hydrofoils, vertical struts, and Wigley ship hulls. A 3D panel method to predict potential flow for yachts was provided by Larson and Janson (1999). In their method, source and doublet were distributed on the lifting part of the yacht. Another numerical method based on Rankine sources was developed for the prediction of flow passing ships by Rigby et al. (2001). Rahmanian (2004) applied the BEM to the hydrodynamic analysis of planing hulls and obtained the induced hydrodynamic lift and drag in steady conditions. Numerical calculations of ship-induced waves using the boundary element method with a triangular mesh surface were conducted by Sadathosseini et al. (2005). Xie et al. (2005) reported a study of the hydrodynamic problem of 3D planing hulls by using the vortex theory and the finite pressure element approach. Bal (2008) and Uslu and Bal (2008) used the boundary element to study hydrodynamic characteristics of 2- and 3D bodies beneath the free surface, and Trafdar and Suzuki (2007) applied a similar method to the study of catamaran vessels. The 3D fully nonlinear waves generated by moving disturbances with steady forward speed without motions were predicted by Kara (2007). Hydrodynamic characteristics of 3D lifting and nonlifting bodies near the free surface were addressed by Ghassemi and Ghiasi (2008). Recently, Kohansal and Ghassemi (2010) presented the numerical modeling of hydrodynamic characteristics of various planing hull forms at small trim angles. A critical aspect in all implementations of the boundary element is an accurate computation of the kernel's integration. When kernels are singular or hypersingular (i.e. when the collocation point belongs to the integration element), a different technique must be devised to achieve proper computation. Several procedures have been proposed to solve these integrals (Gao, 2005; Ghassemi and Kohansal, 2009).

The main purpose of this study was therefore to estimate the hydrodynamic characteristics of the planing hull by using the potential theory and boundary element method. The wetted area of the hull was prescribed and a number of numerical tests were carried out to verify the present method. The validation of the present method was confirmed with good correlation to the experimental data and also with other available numerical results.

Governing Equations

A planing hull was considered to move at a constant speed on unrestricted and calm water, as shown in Figure 1. A right-hand coordinate system, *o-xyz*, was assumed to be located on the planing hull advancing at forward speed U on the undisturbed water surface. The horizontal and vertical axes, *ox* and *oz*, were assumed to be along and at a right angle to the direction of motion, and the y-axis completed the right-handed system. The origin of the coordinate system was located at the base plane of the transom. Traditional ideal flow assumptions that ignore the effect of viscosity and compressibility were utilized. These assumptions led to a boundary value problem for the velocity potential with Laplace's equation satisfied in the fluid. Under the global coordinate system, a total velocity potential $\Phi(x, y, z)$ consists of inflow potential and flow due to the presence of the body, and can be defined as follows:

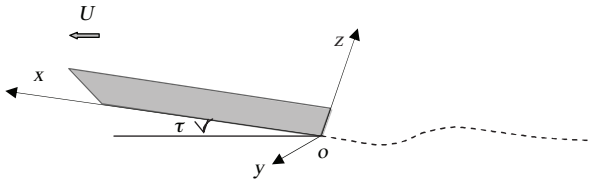

Figure 1. Definition sketch of the coordinate system.

$$\Phi(x,y,z) = \varphi_\infty(x,y,z) + \phi(x,y,z), \tag{1}$$

where $\varphi_\infty(x,y,z) = \vec{U}.\vec{x}$ is the incoming velocity potential and $\vec{x}$ is the position vector, and $\phi(x,y,z)$ is the velocity potential due to the interaction between the inflow potential, the body, and the free surface. Thus, the total potential can be written as follows:

$$\Phi(x,y,z) = \vec{U}.\vec{x} + \phi(x,y,z). \tag{2}$$

Both the total and perturbation velocity potentials are governed by Laplace's equation in domain Ω:

$$\nabla^2\Phi = \nabla^2\phi = 0. \tag{3}$$

The following boundary conditions should also be satisfied:

$$\frac{\partial\Phi}{\partial n} = 0 \quad \Rightarrow \quad \frac{\partial\phi}{\partial n} = -\vec{U}.\vec{n} \text{ on } S_B, \tag{4}$$

$$\begin{cases} \frac{\partial\Phi}{\partial x}.\frac{\partial\zeta}{\partial x} + \frac{\partial\Phi}{\partial y}.\frac{\partial\zeta}{\partial y} - \frac{\partial\Phi}{\partial z} = 0 \text{ on } z = \varsigma, \\ g\zeta + \frac{1}{2}(\nabla\Phi.\nabla\Phi - U^2) = 0 \text{ on } z = \varsigma, \end{cases} \tag{5}$$

$$g\frac{\partial\Phi}{\partial z} + \nabla\Phi.\nabla(\frac{1}{2}\nabla\Phi.\nabla\Phi) = 0 \text{ on } z = \varsigma, \tag{6}$$

$$\phi_{xx} - K_0\Phi_z = 0 \text{ on } S_F, \tag{7}$$

$$\Phi(x,y,z) \to x \cdot \vec{U} \text{ far away upstream.} \tag{8}$$

The potential ϕ is calculated by the boundary element method, which is based on Green's identity. Let us consider a closed computational domain Ω with boundary S and unit normal vector $\hat{n}$ to S, and oriented into Ω, as depicted in Figure 2. In general, the boundary surface includes the body surface (S_B) and the free surface (S_F). Thus, the perturbation potential ϕ is given by the following integral expression with points q (source point) on S and p (field point) in domain Ω:

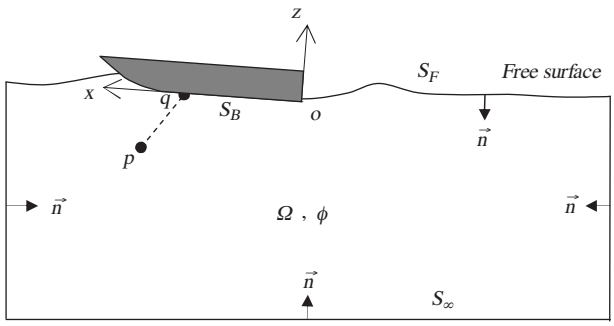

Figure 2. Definition of the coordinate system and notation.

$$4\pi\, e\, \phi(P) = \int\limits_{S_B} \left[\phi(q)\frac{\partial G}{\partial n_q} - \frac{\partial \phi(q)}{\partial n_q} G\right] dS - \int\limits_{S_F} \left[\frac{\partial \phi(q)}{\partial n_q} G\right] dS, \tag{9}$$

where $\partial/\partial n$ is the normal derivative with respect to point q. Meanwhile, e is the solid angle and can be defined as follows:

$$e = \begin{cases} 1/2 \text{ for } P \text{ on } S_B, \\ 1 \text{ for } P \text{ on } S_F. \end{cases} \tag{10}$$

G is Green's function, which might be expressed in the form $G = 1/R_{pq} + 1/R'_{pq}$. Here R_{pq} is the distance between the field point p and the source point q $\left(R_{pq} = \sqrt{(x-\xi)^2 + (y-\eta)^2 + (z-\zeta)^2}\right)$, and R'_{pq} is the distance between the field point p and the image of the source point relative to the mean free surface $\left(R'_{pq} = \sqrt{(x-\xi')^2 + (y-\eta')^2 + (z-\zeta')^2}\right)$, where (ξ, η, ζ) and (ξ', η', ζ') are coordinates of points q and q', respectively. Therefore, Eq. (9) can be expressed as:

$$\begin{aligned} 4\pi e\phi(p) = &\int\limits_{S_B} \phi(q)\frac{\partial}{\partial n_q}\left(\frac{1}{R_{pq}} + \frac{1}{R'_{pq}}\right) dS - \int\limits_{S_B} \frac{\partial \phi(q)}{\partial n_q}\left(\frac{1}{R_{pq}} + \frac{1}{R'_{pq}}\right) dS \\ &- \int\limits_{S_F} \frac{\partial \phi(q)}{\partial n_q}\left(\frac{1}{R_{pq}} + \frac{1}{R'_{pq}}\right) dS \end{aligned}. \tag{11}$$

Numerical Scheme

The body surface and the free surface were discretized into the quadrilateral elements (Figure 3). The discretized form of integral Eq. (11) for the body and free surface are expressed as:

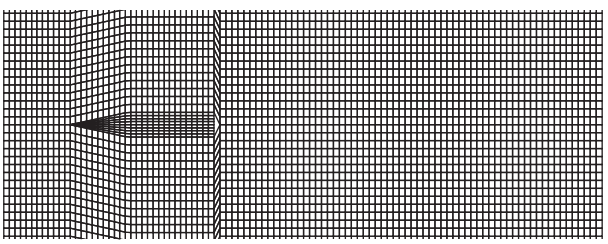

Figure 3. Element arrangement of the craft and free surface domain.

$$\sum_{j=1}^{N_B} \left[\delta_{ij} - \bar{C}_{ij}\right] \{\phi_j\} - \sum_{j=1}^{N_B} [B_{ij}] \left\{(\partial\phi/\partial n)_j\right\} + \sum_{j=1}^{N_F} [F_{ij}] \left\{(\partial\phi/\partial n)_j\right\} = 0, \qquad i = 1, 2, .., N_B \tag{12}$$

$$\begin{aligned} &\sum_{j=1}^{N_B} \frac{\partial^2[\bar{C}_{ij}]}{\partial x^2} \{\phi_{xxj}\} - \sum_{j=1}^{N_B} \frac{\partial^2[B_{ij}]}{\partial x^2} \left\{(\partial\phi_{xx}/\partial n)_j\right\} + \sum_{j=1}^{N_F} \left(\frac{\partial^2[F_{ij}]}{\partial x^2} - K_0\delta_{ij}\right) \left\{(\partial\phi_{xx}/\partial n)_j\right\} = 0, \\ &i = 1, 2, .., N_F \end{aligned}. \tag{13}$$

Here, N_B and N_F are the number of elements on the body and the free surfaces, respectively, and $\bar{C}_{ij}$ and B_{ij} are the influence coefficients on element j acting on the control point of element i.

$$\bar{C}_{ij} = \frac{1}{4\pi e} \int\limits_{S_B} \frac{\partial}{\partial n_j} \left(\frac{1}{R_{pq}} + \frac{1}{R'_{pq}} \right) dS_j, \tag{14}$$

$$B_{ij} = \frac{1}{4\pi e} \int\limits_{S_B} \left(\frac{1}{R_{pq}} + \frac{1}{R'_{pq}} \right) dS_j. \tag{15}$$

$$F_{ij} = \frac{1}{4\pi e} \int\limits_{S_F} \left(\frac{1}{R_{pq}} + \frac{1}{R'_{pq}} \right) dS_j, \tag{16}$$

The combination matrix form of Eqs. (12) and (13) are expressed as either

$$\begin{bmatrix} [\delta - \bar{C}]_{N_B \times N_B} & [F]_{N_B \times N_F} \\ [\bar{C}_{xx}]_{N_F \times N_B} & [-K_0\delta + F_{xx}]_{N_F \times N_F} \end{bmatrix} \begin{Bmatrix} \{\phi\}_{N_B \times 1} \\ \{\sigma\}_{N_F \times 1} \end{Bmatrix} = \begin{bmatrix} [B]_{N_B \times N_B} \\ [B_{xx}]_{N_F \times N_B} \end{bmatrix} \begin{Bmatrix} \{\vec{U}.\vec{n}\}_{N_B \times 1} \\ \{0\}_{N_F \times 1} \end{Bmatrix} \tag{17}$$

or

$$[A]_{N_T \times N_T} \{x\}_{N_T \times 1} = \{b\}_{N_T \times 1}, \tag{18}$$

where δ_{ij} is the Kronecker delta function. The velocity component $(\partial\phi/\partial n)_j$ and potential ϕ_j are considered to be linear on the j^{th} element. For this type of problem, a formal solution may be given by the direct methods of LU decomposition.

Velocity and pressure distribution

A local distribution of the potential was considered on 5 elements, and the tangential velocity was computed by derivation. s_2 and s_1 were defined by connecting the middle points of element sides. a_1 and a_2 are the local orthogonal coordinates. a_1 and s_1 are in the same direction, and a_2 is normal to a_1 (Figure 4). e_1, e_2, and t_2 are the unit vectors in a_1, a_2, and s_2 directions, respectively. The velocity potential in the local orthogonal coordinate system can be expressed as:

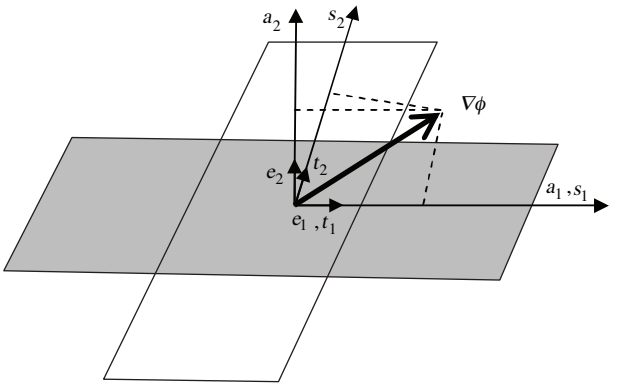

Figure 4. Local element and adjacent elements.

$$\phi = as^2 + bs + c. \tag{19}$$

Therefore, the velocity can be computed as:

$$\nabla\phi = \vec{v}_t = \frac{\partial\phi}{\partial a_1}\vec{e}_1 + \frac{\partial\phi}{\partial a_2}\vec{e}_2. \tag{20}$$

From Figure 4, it is apparent that the velocity components in a_1 and s_1 directions are the same, while the velocity components in a_2 and s_2 directions are different. It can be written as:

$$\frac{\partial\phi}{\partial a_1} = \frac{\partial\phi}{\partial s_1} \tag{21}$$

$$\frac{\partial\phi}{\partial a_2} = \frac{\frac{\partial\phi}{\partial s_2} - (\vec{t}_2.\vec{e}_1)\frac{\partial\phi}{\partial s_1}}{(\vec{t}_2.\vec{e}_2)}, \tag{22}$$

and then:

$$\nabla\phi = \vec{v}_t = \frac{\partial\phi}{\partial s_1}\vec{e}_1 + \frac{\frac{\partial\phi}{\partial s_2} - (\vec{t}_2.\vec{e}_1)\frac{\partial\phi}{\partial s_1}}{(\vec{t}_2.\vec{e}_2)}\vec{e}_2. \tag{23}$$

The induced velocity around the body may be determined by direct differentiation of Eq. (11) for $e(p) = 1$, giving:

$$4\pi \cdot \vec{V}_i(P) = \int\limits_{S_B+S_F} \phi(q)\nabla_P \left[\frac{\partial}{\partial n_q}\left(\frac{1}{R_{pq}} + \frac{1}{R'_{pq}}\right)\right] dS_q - \int\limits_{S_B+S_F} \frac{\partial\phi(q)}{\partial n_q}\nabla_P \left[\frac{1}{R_{pq}} + \frac{1}{R'_{pq}}\right] dS_q, \tag{24}$$

where

$$\nabla_P = \frac{\partial}{\partial n_{Px}}\vec{i} + \frac{\partial}{\partial n_{Py}}\vec{j} + \frac{\partial}{\partial n_{Pz}}\vec{k}. \tag{25}$$

The arbitrary domain around the body was discretized into N_{Field} points. Thus, the discretization form of Eq. (24) is expressed for a given point p_i on S as:

$$\vec{V}_i(P) = \sum_{j=1}^{N} \phi^j \nabla_P D_{ij} - \sum_{j=1}^{N} \phi_n^j \nabla_P S_{ij}, i = 1, 2, .., N_{Field}, \tag{26}$$

where:

$$\begin{cases} \nabla_P D_{ij} = \frac{1}{4\pi} \sum\limits_{k=1}^{k} \int\limits_{S_J} \nabla_P \left[\frac{\partial}{\partial n_j}\left(\frac{1}{R_{pq}} + \frac{1}{R'_{pq}}\right)\right] dS_J \\ \nabla_P S_{ij} = \frac{1}{4\pi} \sum\limits_{k=1}^{k} \int\limits_{S_J} \nabla_P \left(\frac{1}{R_{pq}} + \frac{1}{R'_{pq}}\right) dS_J \end{cases}. \tag{27}$$

The integrals involved in the above equations were numerically calculated by the Gauss quadrature integration method. The pressure on the hull surface was calculated by Bernoulli's equation in the following way:

$$\frac{P}{\rho} = -gz - \frac{1}{2}\nabla\phi \cdot \nabla\phi = -\left(gz + \left(\frac{1}{2}\nabla\phi - \vec{U}\right) \cdot \nabla\phi\right), \tag{28}$$

or

$$P = -\rho g\, h_z + \ 0.5\rho \left(2\,\vec{U}.\,\vec{v}_t - \vec{v}_t.\,\vec{v}_t\right). \tag{29}$$

The first term in the right part of Eq. (29) is the hydrostatic pressure, P_h, and h_Z is the immersed part of the hull surface position. The second term is the dynamic part of pressure P_d, which is generated by the induced velocity. After calculating fluid velocity $\nabla\Phi$ on the body surface, the pressure coefficient can be assessed as:

$$C_P = 1 - \left(\frac{\nabla\Phi}{U}\right)^2 = 1 - \left(1 - \frac{\nabla\phi}{U}\right)^2. \tag{30}$$

Hydrodynamic forces

The hydrodynamic lift forces (L_d), buoyant force (L_s), and induced drag (D_i) acting on the hull can be obtained by integrating the pressure over the entire wetted surface:

$$\begin{aligned} L_d &= 0.5\rho \int\limits_{S_B} \left(2\vec{U}.\vec{v}_t - \vec{v}_t.\vec{v}_t\right) n_z dS \\ L_s &= \int\limits_{S_B} \rho g h_z dS \\ D_i &= 0.5\rho \int\limits_{S_B} \left(2\vec{U}.\vec{v}_t - \vec{v}_t.\vec{v}_t\right) n_x dS \end{aligned}, \tag{31}$$

where $\vec{n}(n_x, n_y, n_z)$ is the outward unit normal vector on the wetted body surface. The total drag (D_T) of a planing hull is made up of several components, i.e. spray drag D_{Spray}, induced drag D_i, and frictional drag D_F:

$$D_T = D_{Spray} + D_i + D_F. \tag{32}$$

At low speeds, the drag is almost frictional. Water surface disturbance of a planing hull can be presented as follows (Bowles and Denny, 2005):

$$L_K - L_C = \frac{B}{2}\frac{\tan\beta}{\tan\tau}(1/(1/(1+\tan(\beta)\tan(\beta/2))^{0.5}+1). \tag{33}$$

The flow velocity component normal to the keel is $U = V_S \sin\tau$. The spray surface area and the pressure due to spray may be approximated by the following equations (Figure 5):

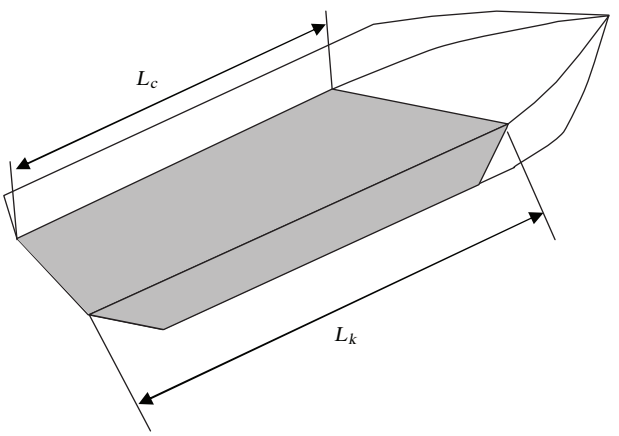

Figure 5. Bottom view of wetted surface area for a craft.

$$A_{Spray} = K_1(L_K - L_C)B/\cos\beta \tag{34}$$

$$P_S = K_2.P(\text{at bow of the } keel), \tag{35}$$

where K_1 and K_2 depend on the hull speed and hull dimensions and are given as follows:

$$\begin{aligned} K_1 = f(Fn_\nabla) &= \begin{cases} 0.2 & \text{if} \quad Fn_\nabla < 3 \\ 0.4 & \text{if} \quad 3 \le Fn_\nabla < 5 \\ 0.7 & \text{if} \quad Fn_\nabla \ge 5 \end{cases} \\ K_2 = f(\beta, \tau, b(y)) &= \begin{cases} 2 & \text{if} \quad b(y) < 0.5B \\ 1.5 & \text{if} \quad 0.5B \le b(y) < 0.9B \\ 1.2 & \text{if} \quad 0.9B \le b(y) \le B \end{cases} \end{aligned} . \tag{36}$$

P is the pressure obtained from Eq. (29) at the nearest element to the spray root, and B and $b(y)$ are the maximum breadth and distance between the spray root and centerline, respectively. The spray drag (D_{Spray}) and lift (L_{Spray}) generated by the spray are estimated separately with the following equations:

$$\begin{aligned} D_{Spray} &= P_S A_{Spray} \cos\tau \\ L_{Spray} &= P_S A_{Spray} \sin\tau \end{aligned} . \tag{37}$$

For each element in the longitudinal stripwise of the hull, the section frictional drag D_F is obtained by:

$$D_F = 0.5\rho \int_0^{l_{wet(j)}} C_f U_e^2 dx = 0.5\rho \sum_{k=1}^{N_{Strip}} C_f U_e^2 (\Delta x), \tag{38}$$

where C_f is the local frictional coefficient and is determined by the ITTC empirical formula (Bertram 2000). N_{Strip} is the number of strips in the longitudinal direction. The forces acting on a planing hull are shown in Figure 6. Vertical plane force equilibrium requires:

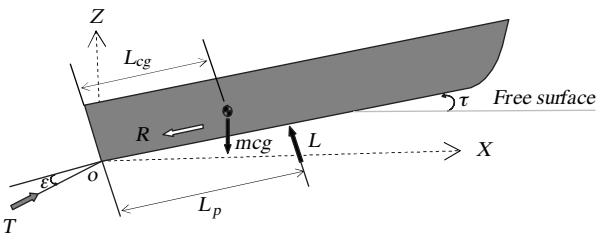

Figure 6. Forces acting on a craft.

$$D_i + D_F + D_{spray} = T\cos(\tau + \alpha_s), \tag{39}$$

$$L_i + L_s + L_{spray} = T\sin(\tau + \alpha_s) = \Delta. \tag{40}$$

Here, T is the propeller thrust and Δ is the vessel weight. The trim angle, τ, is defined as the angle between the undisturbed free surface and a line tangent to the keel at the keel-transom intersection. The shaft angle, α_s, is also measured from a line tangent to the keel at the keel-transom intersection and shaft centerline.

Wave pattern

When the body (hull) moves, it produces wave patterns. The movement of a body across the free surface of water creates a variable pressure distribution along the body. The pressure variation generates a set of waves that move out away from the body. The far-field wave pattern created by a body moving at a constant speed on a straight course in still and deep water consists of diverging and transverse waves. The computation of the steady wave patterns generated by a planing hull moving at a constant forward speed U is a matter of high interest for naval architects and marine and ocean engineers. The design and location of propulsion inlets, cooling water inlets, propellers, rudders, etc. are all influenced by the shape of the planing hull and the waves generated around it. The waves may affect other bodies and cause nearby small boats to capsize or ground, or may cause large moored ships to move and mooring lines to break. The wave patterns generated by a planing hull will affect the design parameters, such as propulsion system arrangements. The accuracy of the estimation of the wave wake in the vicinity of a planing hull is essential for the calculation of the pressure distribution under the bottom of the hull and then for the prediction of the hydrodynamics of the planing hull. At moderate speeds, planing hulls produce bow waves, which increase their drag but have little effect on lift. At high speeds, the hull is lifted out of the water and starts planing, so the wave-making drag is considerably reduced. At larger Froude numbers, the transverse waves tend to disappear, so, in the far field, where the Froude number is large, the wave pattern is dominated by divergent waves. The expression for free surface elevation $\varsigma(x, y)$ can be obtained by inserting potential velocity $\phi(x, y, z)$into the free surface condition (Eq. 7). The wave profile can be obtained by:

$$\zeta = -\frac{U}{g}\frac{\partial \phi}{\partial x} \text{ on } S_F. \tag{41}$$

Numerical Results

Planing hull

A number of numerical tests were carried out to verify the method. Calculations were made for a number of V-shape hulls with different deadrise angles, wetted length-to-beam ratios, and Froude numbers during pure planing to compare the results with those of Kapryan and Boyd (1955). First of all, the effect of the free surface on the pressure distribution of the planing hull is shown in Figure 7 for a 20° deadrise angle at $Fn = 1.20$. For several related prismatic planing hulls, with deadrise angles of 20° and 40°, the pressure distributions were computed during pure planing and are presented for various wetted length-to-beam ratios and trim angles. To compare calculated nondimensional pressure distribution values (Cp) on V-shaped planing hulls with experimental ones, several planing hulls with different deadrise angles ($\beta = 20^0$ and $, 40^0$), trim angles ($\tau = 6^\circ$, 9°, 18°, 30°), and length-to-beam ratios ($L/B = 0.87$, 1.02, 2.52) were chosen and some results are presented in Figures 8-13. The effects of varying wetted length-to-beam ratio and trim angle on pressure distribution coefficients (and, consequently, on the lift and drag coefficients) are given in these Figures. The reduction in pressure accompanying an increase in the angle of the deadrise was about what would be expected on the basis of experimental data. These Figures reveal that for a fixed Froude number, as the trim angle is increased, the value of Cp increases, and at higher values of the deadrise angle, the value of Cp decreases. For a fixed deadrise angle and a decreasing length-to-beam ratio (L/B), the nondimensional pressure increases. In general, the high- and low-pressure areas are virtually identical, although the numerical pressures in the vicinity of the stagnation point are seen to be higher than those predicted by experiments. It is clear that, although the trends are the same, the numerical method predicts larger values in this region. Certainly, the experimental

accuracy also plays an important role in these discrepancies. Figure 14 presents the wave contours produced by a planing hull with and without a trim angle at $Fn = 1.20$. As can be seen, diverging waves spread out from the bow and transverse waves follow behind the hull. The trim and rise of the center of gravity (CG) is shown in Figure 15. When the Froude number (Fn) increases, the trim diminishes and the rise of the CG increases.

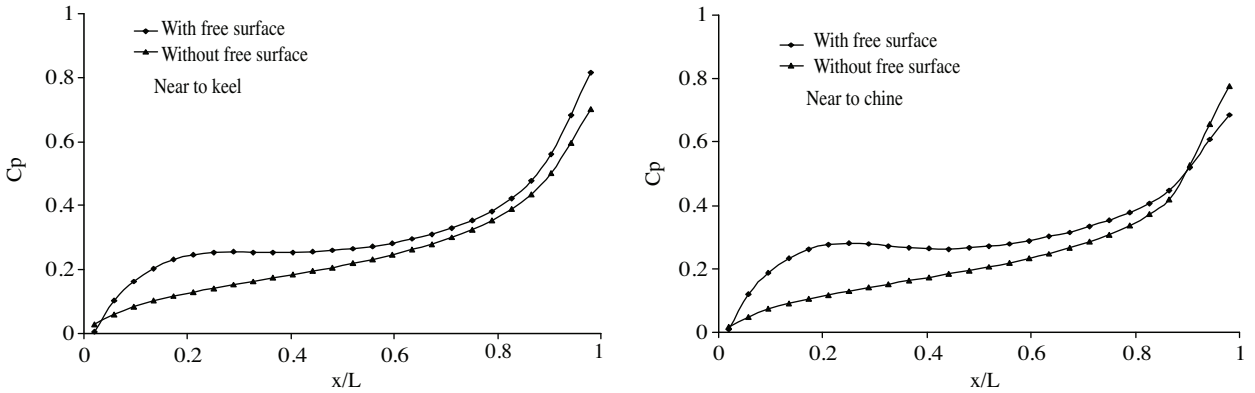

Figure 7. Comparison of pressure distribution on a 20° deadrise angle of the hull at $Fn = 1.20$ with and without the free surface effects.

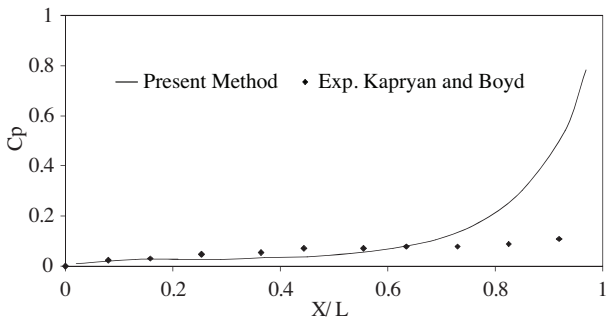

Figure 8. Nondimensional pressure distribution on a planing hull ($Deadrise = 20^{\bigcirc}, U = 12.17\ [m/s]$, $Trim = 6^{\circ}$, $L/B = 0.86$).

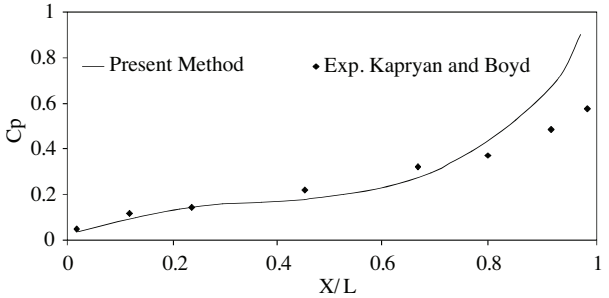

Figure 9. Nondimensional pressure distribution on a planing hull ($Deadrise = 20^{\circ}, U = 12.17\ [m/s]$, $Trim = 18^{\circ}$, $L/B = 1.02$).

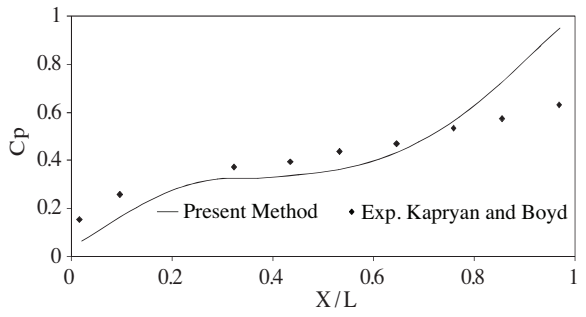

Figure 10. Nondimensional pressure distribution on a planing hull ($Deadrise = 20^{\circ}, U = 12.17\ [m/s]$, $Trim = 30^{\circ}$, $L/B = 1.02$).

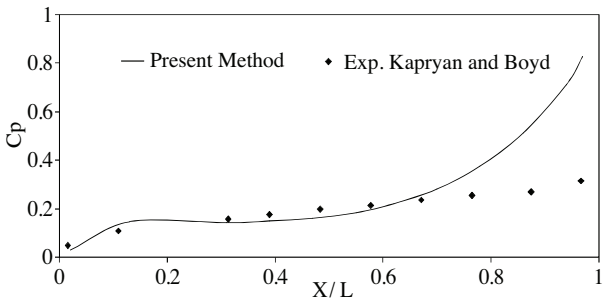

Figure 11. Nondimensional pressure distribution on a planing hull ($Deadrise = 40^{\circ}, U = 12.17\ [m/s]$, $Trim = 18^{\circ}$, $L/B = 0.98$).

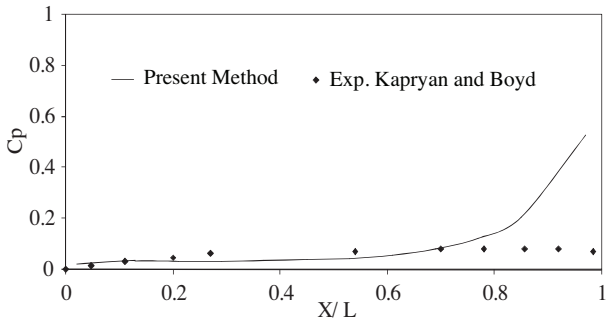

Figure 12. Nondimensional pressure distribution on a planing hull ($Deadrise = 40\,^{\circ}, U = 12.17\ [m/s]$, $Trim = 9^{\circ}$, $L/B = 2.52$).

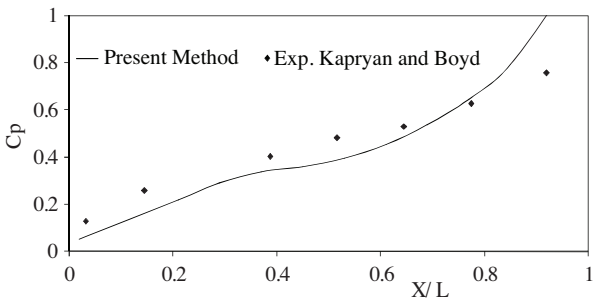

Figure 13. Nondimensional pressure distribution on a planing hull ($Deadrise = 40^{\circ}, U = 12.17\ [m/s]$, $Trim = 30\,^{\circ}$, $L/B = 2.52$).

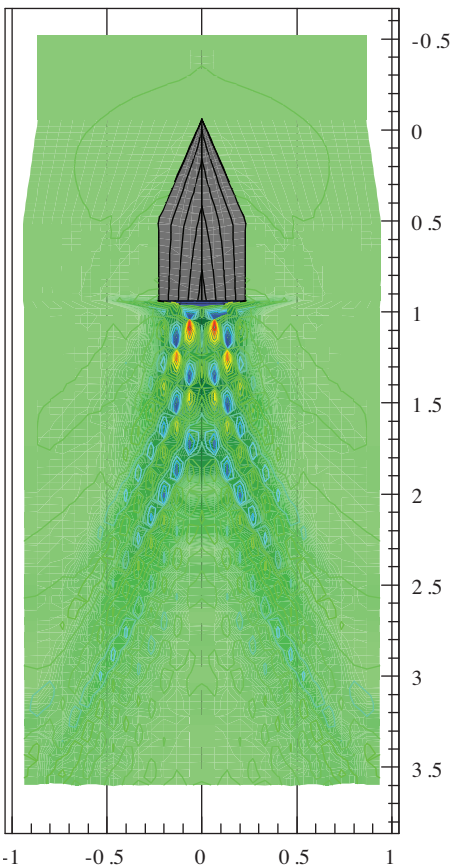

Figure 14. Wave contours for a planing hull with a 20° deadrise angle at $Fn = 1.20$, $\tau = 10^{\circ}$.

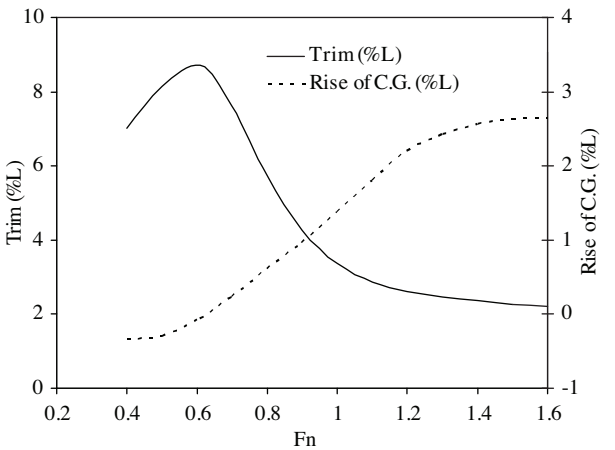

Figure 15. Trim and rise of CG (as percentage of length) in terms of Froude number.

Planing wedge-shape

The present method was extended to a planing wedge-shaped hull. This hull was defined as $z = f(x, y) = (y/B - x/L) \cdot h$ and $z < 0$. Its overall length, L, is 0.754, the maximum hull breadth $B = 0.786$, the hull depth

at the transom stern $h = 0.085$, the deadrise angle $\beta = 13^\circ$, and the trim angle $\tau = 6^\circ$. Figure 16 illustrates a 3D view of this hull. In numerical computations, the effects of spray on the drag, lift, and moment are considered. Convergence of lift and drag coefficients of a planing wedge-shape versus the number of elements at $Fn = 1.2$ are shown in Figure 17. We found that the solutions presented here were independent of the number of the elements if we choose more than 2000 elements on the body and free surface. Elements were also arranged in equal spacing forms; the elements on the body and free surface should not be very different in dimensions. Figure 18 shows a comparison of drag coefficient values $\left(C_D = D \Big/ \rho U^2 \nabla^{2/3}\right)$ for a planing wedge-shaped hull in different Froude numbers with the experimental results presented by Himeno et al. (1993). The spray drag is important at high speeds. This component is predicted by empirical formulae, as shown in Eq. (36). At low speeds ($Fn < 0.5$), no spray drag appears, while at high speeds ($Fn > 1$), this component may be considerable. It is shown that with the present calculations, this component is about 5%-8% of the total drag. In Figure 19, the coefficients of the hydrodynamic lift $\left(C_L = L \Big/ \rho U^2 \nabla^{2/3}\right)$ exerted on the bottom of this hull, which are obtained by the integration of the pressure distribution, are compared with those obtained from the force measurements. The hydrodynamic lift and drag increase as the Froude number is increased from 0, and a maximum is reached at about $Fn = 1.20$. These forces then decrease as the Froude number is increased further. A comparison of the moment about a horizontal axis through transom for the planing wedge-shaped hull against the Froude number is given in Figure 20. As can be seen from these figures, the calculated results are somewhat underpredicted. It was found that by consideration of spray effects on the bow region of the planing hull, better agreement with the experimental results could be achieved. Agreement between the present method and experimental results was shown to be good. Some discrepancies were noted near the stern, where separation and eddy losses may be present in the experiment. The wave contours for planing wedge-shaped hulls at $Fn = 1.20$ predicted by the present method are given in Figure 21. In general, it was found that the presented numerical results are in good agreement with the experimental data, and it seems that this method is efficient and applicable for predicting the hydrodynamic performance of 3D planing hulls and planing wedge-shapes.

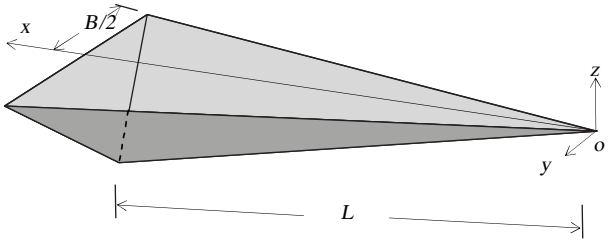

Figure 16. Three-dimensional view of a planing wedge-shaped hull.

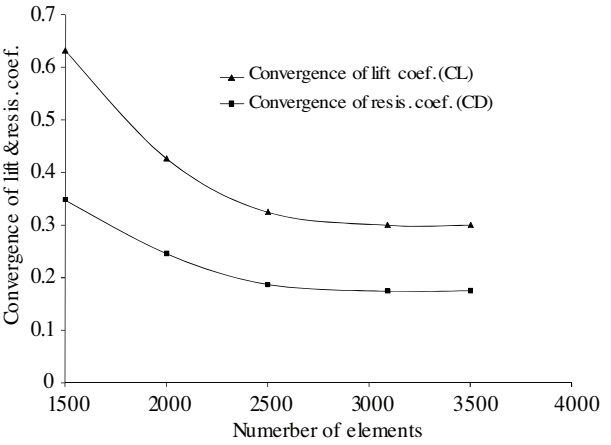

Figure 17. Convergence of lift and drag coefficients of planing wedge-shape versus the number of elements, $Fn = 1.2$.

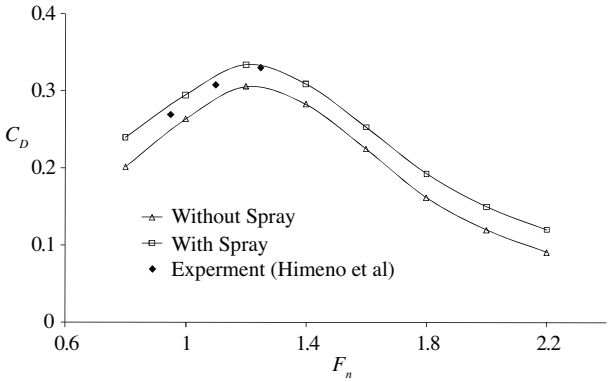

Figure 18. Drag coefficient for a planing wedge-shaped hull against Froude number Fn, with and without spray effect.

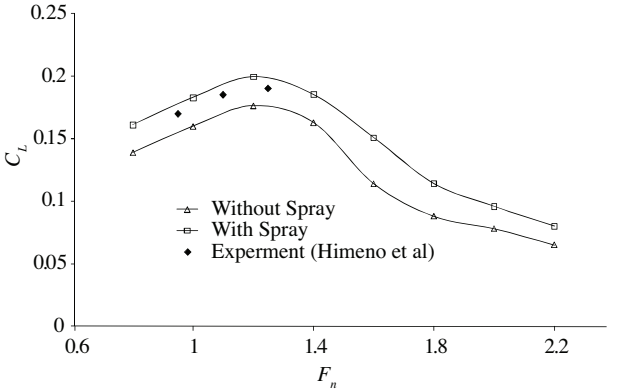

Figure 19. Hydrodynamic lift coefficient for a planing wedge-shaped hull against Fn, with and without spray effect.

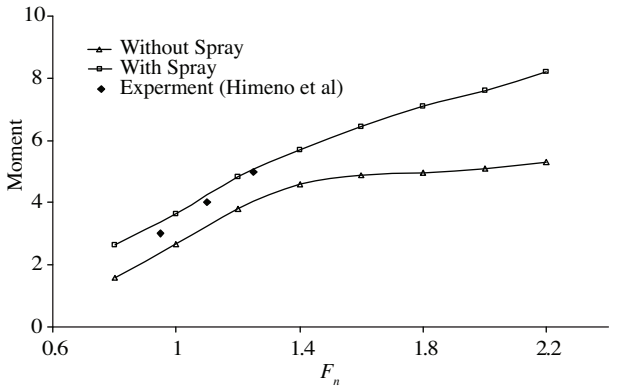

Figure 20. Moment about a horizontal axis through transom for a planing wedge-shaped hull against Fn, with and without spray effect.

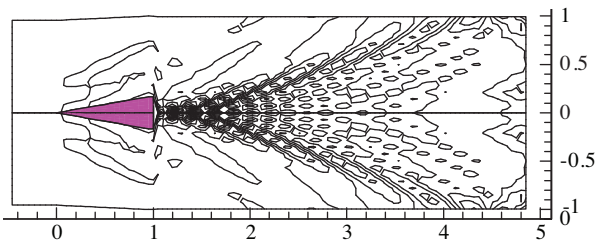

Figure 21. Wave contours for a planing wedge-shaped hull at $Fn = 1.20$.

Conclusion

In this paper, prediction of hydrodynamic characteristics of planing hulls and wedge-shapes was performed by means of the boundary element method. Numerical computations were conducted in this study for various 3D planing hulls, and pressure distributions were calculated numerically for a series of related planing hulls at different deadrise angles, wetted length-to-beam ratios, and Froude numbers. The wave-making phenomenon of planing hulls was also modeled by the present method. Comparison was made with experimental data and other authors' results, as well, and the good agreement between the 2 types of results verifies the reliability and accuracy of the present numerical schemes in achieving converged solutions without imposing any restrictions on either the aspect ratio or Froude number. On the whole, the present numerical method constitutes a useful tool for a conceptual and preliminary design of planing hulls. With a few modifications, this method could also be applied to different hull forms of planing crafts.

Nomenclature

A_{spray}	spray area
B	breadth of the hull
$b(y)$	distance between spray root and centerline
C_P	pressure coefficient
C_L	lift coefficient
C_f	local frictional coefficient
e	solid angle
Fn	length Froude number
F_∇	volumetric Froude number
g	gravitational acceleration
h_z	element immersion
G	Green's function
K_0	wave number
L	length of the hull
L_c	chine wetted length
L_i	hydrodynamic lift
L_k	keel wetted length
L_s	hydrostatic lift
L_{spray}	spray lift
N_B	total number of elements on the body
N_F	total number of elements on the free surface
N_T	total number of elements
$\vec{n}(n_x, n_y, n_z)$	outward unit normal vector
P	pressure
P_S	spray pressure
R_i	induced drag
R_F	frictional drag
R_{pq}	distance between the singular point p to integration point q
R'_{pq}	distance between the singular point p to image integration point q′
R_{Spray}	spray drag
R_T	total drag
S_B	surface of the body
S_F	surface of the free surface
$\bar{C}_{ij}, B_{ij}$	influence coefficient of source, double on the body
F_{ij}	influence coefficient of double and source on the free surface
T	thrust of the propeller
$\vec{U}$	inflow velocity
(u, v, w)	local coordinate system
$\vec{v}_t$	induced velocity
$\vec{X}(p)$	position vector
(x, y, z)	global coordinate system

Greek Symbols

α_s	shaft angle
β	deadrise angle
ϕ	perturbation potential
φ_∞	free stream velocity potential
ϕ_{xx}	second derivative of the potential in x-direction
$\Phi(x, y, z)$	total velocity potential
Φ_x, Φ_y, Φ_z	derivative of velocity potential relative to x-, y-, and z-directions
$\partial\phi/\partial n$	normal derivative of the velocity potential
$\zeta(x, y)$	wave elevation
(ξ, η, ζ)	coordinates of point q
(ξ', η', ζ')	coordinates of point q'
δ_{ij}	Kronecker delta function
σ	source strength on each free surface element
ρ	density of the water
τ	trim angle
$\nabla\phi$	differentiation of potential
Δ	weight of the hull

Acknowledgment

This research was financially supported by the Marine Research Center of Amirkabir University of Technology. Furthermore, Dr. Mohammad Movahhed of Persian Gulf University is acknowledged for his help in revising the manuscript.

References

Bal, S., "Prediction of Wave Pattern and Wave Resistance of Surface Piercing Bodies by a Boundary Element Method", International Journal for Numerical Methods in Fluids, 56, 305-329, 2008.

Bertram, V., "Practical Ship Hydrodynamics", Butterworth-Heinemann, Oxford, 2000.

Bowles, B.J and Denny, B.S., "Water Surface Disturbance Near The Bow of High Speed, Hard Chine Hull Forms", 8th International Conference on Fast Sea Transportation (FAST), St. Petersburg, Russia, 2005.

Cao, Y., Schultz, W.W. and Beck, R.F., "Three-Dimensional Desingularized Boundary Integral Methods for Potential Problems", International Journal for Numerical Methods in Fluids, 12, 785-803, 1991.

Dawson, D.W., "A Practical Computer Method for Solving Ship-Wave Problems", Proceedings of the 2nd International Conference on Numerical Ship Hydrodynamics, USA, 1977.

Gao, X.W., "Evaluation of Regular and Singular Domain Integrals with Boundary-Only Discretization Theory and Fortran Code", Journal of Computational and Applied Mathematics, 175, 265-290, 2005.

Ghassemi, H. and Ghiasi, M., "A Combined Method for the Hydrodynamic Characteristics of Planing Crafts", Ocean Engineering, 35, 310-32, 2008.

Ghassemi, H. and Kohansal, A.R., "Numerical Evaluation of Various Levels of Singular Integrals, Arising in BEM and its Application in Hydrofoil Analysis", Applied Mathematics and Computation, 213, 277-289, 2009.

Himeno, Y., Hirano, S. and Kitagawa, K., "Wave Characteristics of Water-Surface Planing Hull Form", J. Kansai Society of Naval Architects and Ocean Engineers, Japan, 220, 1993.

Hsin, C.Y. and Chou, S.K., "Applications of a Hybrid Boundary Element Method to the Analysis of Free Surface Flow Around Lifting and Nonlifting Bodies", Proceedings of the 22nd Symposium on Naval Hydrodynamics, Washington DC, 1998.

Janson, C.E., "Potential Flow Panel Method for the Calculation of Free Surface Flows with Lift", PhD Dissertation, Chalmers University of Technology, 1997.

Kapryan, W.J. and Boyd, G.M., "Hydrodynamic Pressure Distributions Obtained During a Planing Investigation on Five Related Prismatic Surfaces", National Advisory Committee for Aeronautics (NACA), Technical Note, 3477, 1955.

Kara, F., Tang, C.Q. and Vassalos, D., "Time Domain Three-Dimensional Fully Nonlinear Computations of Steady Body-Wave Interaction Problem", Ocean Engineering, 34, 776-789, 2007.

Kohansal, A.R. and Ghassemi, H., "A Numerical Modeling of Hydrodynamic Characteristics of Various Planing Hull Forms", Ocean Engineering, 37, 498-510, 2010.

Larson, L. and Janson, C.E., "Potential Flow Calculations for Sailing Yachts", CFD for Ship and Offshore Design, 31st WEGMENT School, Hamburg, 1999.

Lee, S.J. and Joo, Y.R., "Calculation of Wave Making Resistance of High Speed Catamaran Using a Panel Method", Proceedings of Third Korea-Japan Joint Workshop on Ship and Marine Hydrodynamics, 1996.

Nakos, D.E. and Sclavounos, P.D., "Kelvin Wakes and Wave Resistance of Cruiser- and Transom-Stern Ships", Journal of Ship Research, 38, 9-29, 1994.

Rahmanian, A., "Computational Analysis of Planing Hull Using BEM", Master Thesis, Department of Marine Technology, Amirkabir University of Technology, 2004.

Rigby, S.G., Nicolaou, D., Sproston, J.L. and Millward, A., "Numerical Modeling of the Water Flow Around Ship Hulls", Journal of Ship Research, 45, 85-94, 2001.

Sadathosseini, S.H., Mousaviraad, S.M. and Seif, M.S., "Numerical Calculations of Ship Induced Waves", Journal of Marine Engineering (IRANAME), 1, 37-47, 2005.

Tarafder, S. and Suzuki, K., "Computation of Wave-Making Resistance of a Catamaran in Deep Water Using a Potential-Based Panel Method", Ocean Engineering, 34, 1892-1900, 2007.

Uslu, Y. and Bal, S., "Numerical Prediction of Wave Drag of 2-D and 3-D Bodies under or on a Free Surface", Turkish Journal of Engineering and Environmental Science, 32, 177-188, 2008.

Xie, N., Vassalos, D. and Jasionowski, A., "A Study of Hydrodynamics of Three-Dimensional Planing Surface", Ocean Engineering, 32, 1539-1555, 2005.

Yasko, M., “Boundary Element Method for a Hydrofoil near the Free Surface”, Engineering Analysis with Boundary Elements, 21, 191-194, 1998.

Zhao R., Faltinsen, O.M. and Haslum, H.A., “A Simplified Nonlinear Analysis of a High-Speed Planing Hull in Calm Water”, Proceedings, 4th Int. Conf. on Fast Sea Transportation, Australia, 1997.